ELSEVIER

Polymer 40 (1999) 7125–7135

polymer

Microscopically viewed structural change of PE during the isothermal crystallization from the melt
II. Conformational ordering and lamellar formation mechanism derived from the coupled interpretation of time-resolved SAXS and FTIR data

Sono Sasaki[a], Kohji Tashiro[a,*], Masamichi Kobayashi[a], Yoshinobu Izumi[b], Katsumi Kobayashi[c]

[a]*Department of Macromolecular Science, Graduate School of Science, Osaka University, Toyonaka, Osaka 560-0043, Japan*
[b]*Graduate School of Engineering, Yamagata University, Yonezawa, Yamagata 992-0038, Japan*
[c]*Institute of Materials Structure Science, High Energy Accelerator Research Organization, Tsukuba, Ibaraki 305-0801, Japan*

Received 27 August 1998; received in revised form 23 October 1998; accepted 10 December 1998

Abstract

Time-resolved small-angle X-ray scattering (SAXS) measurement was carried out to trace the structural change of polyethylene (PE) during the isothermal crystallization from the melt. All kinds of PE samples of high-density PE, linear low-density PE, and deuterated high-density PE were found to show essentially the same SAXS pattern changes, although the crystallization rates were different among them. The thus obtained SAXS data were combined with the previously reported FTIR data [Tashiro K., Sasaki S., Kobayashi M., Polym J, 1998;30:485] and could be interpreted quantitatively by dividing into the following three time regions: (1) immediately after the sample was cooled to the crystallization temperature, the density fluctuation in the molten state increased, resulting in the generation of the conformationally disordered short *trans* segments. (2) The disordered *trans* segments experienced the conformational ordering to the orthorhombic-type *trans*-zigzag form. These regular chain segments were aggregated to form a crystalline lamella of ca. 50 Å thickness. This separation of the system into the high (lamella) and low density (amorphous) regions occurred with ca. 800 Å period. (3) These isolated lamellae were stacked more densely by generating new lamellae in between the already existing lamellar layers, creating a structure of ca. 400 Å period.

Keywords: Polyethylene; Isothermal crystallization; Time-resolved SAXS

1. Introduction

When the crystalline polymer is slowly cooled from the melt, a spherulite is created. In the spherulite the crystalline lamellae and the amorphous phase are aggregated together to construct the higher-order structure. It is important to clarify this complicated crystallization mechanism from the microscopic molecular level. But the regularization process of the polymer chains from the random coils to the crystalline phase is still under discussion [1]. Polyethylene (PE) is one of the typical examples. PE crystallizes too fast and makes it difficult to trace the structural change in the crystallization process step by step. Recently, the detailed discussion on the PE crystallization has begun to be reported on the basis of the time-resolved small-angle X-ray scattering (SAXS) data measured by using the synchrotron radiation source and/or highly-sensitive detector [1–15]. In most of these studies, however, the temperature jump from the melt to an isothermal crystallization temperature was not so sharp as to allow us to trace the details of the structural change of PE. In other words, the structural information might become obscure because of such a “diffuse” temperature change. Besides the discussion was made mainly on the lamellar structural formation, not about the structural change in the molecular level.

In the previous article, we investigated the ordering process of the chain conformation in the isothermal crystallization process from the melt by carrying out the time-resolved measurements of high-resolution FTIR spectra for linear low-density PE (LLDPE), high-density PE(HDPE), and deuterated HDPE (DHDPE) [16,17]. At the early stage of the isothermal crystallization, the FTIR data showed that the conformationally disordered short *trans* sequences were observed to appear at first in the random coils of the melt and these disordered *trans*

* Corresponding author. Tel.: + 81-6-850-5455; fax: + 81-6-850-5653.
E-mail address: ktashiro@chem.sci.osaka-u.ac.jp (K. Tashiro)

0032-3861/99/$ - see front matter
PII: S0032-3861(98)00864-7

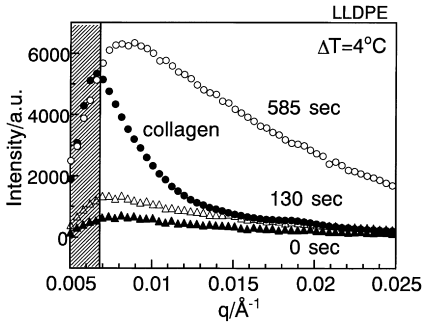

Fig. 1. SAXS profiles of LLDPE measured at the various times in the isothermal crystallization process in comparison with the SAXS profile of a standard sample, collagen. Judging from the SAXS profile of collagen, the data in the q range lower than 0.0068 $Å^{-1}$ can not be used because of the effect of beam stopper.

sequences grew to the longer and more regular *trans* sequences of the orthorhombic-type crystal.

It is quite important to clarify the relation between the conformational ordering of chains and the formation of aggregation structure of lamellae in order to understand the details of the isothermal crystallization mechanism. In the present study, the isothermal crystallization behavior from the melt was traced by the time-resolved small-angle SAXS measurements for PE samples. These data were combined with the previously reported FTIR data [17] and analyzed to obtain the concrete structural change viewed from both the microscopic and macroscopic points.

2. Experimental section

2.1. Samples

The samples used here were those employed in a series of our studies on the cocrystallization phenomena of the blends between the DHDPE and LLDPE with various degree of ethyl branching [18–25]. In the present article we will focus our attention on the samples of LLDPE and DHDPE. Compared with the HDPE sample, the crystallization rate is relatively low for these two samples, making the time-resolved measurements easier. Besides, the essential features of the crystallization behavior are not different very much among all these samples [17,23]. The LLDPE was supplied by Exxon Chemicals Co., Ltd. and the DHDPE was purchased from Merck Chemical Co. Ltd. The characterization of these samples was made as follows:

	M_w	M_n	M_w/M_n	ethyl branching/1000C
LLDPE	75K	37K	2.0	17
DHDPE	107k	34k	3.1	2–3

2.2. Temperature jump and SAXS measurements

The degree of supercooling (ΔT) was defined as $\Delta T = T°m - Tc$, where $T°m$ is the equilibrium melting temperature and Tc is a crystallization temperature. We tried to determine $T°m$ by carrying out the Hoffman–Week's plot [26]. For example, the $T°m$ of LLDPE was evaluated to be ca. 111°C. However, Alamo et al. reported that this method does not necessarily lead to a reasonable equilibrium temperature [27]. Therefore the temperature $T°c$, at which the crystallization bands begin to be observed in the infrared spectral measurement during the slow cooling from the melt [20–25], was used tentatively instead of the $T°m$. That is to say, ΔT was re-defined as $\Delta T = T°c - Tc$.

PE crystallizes rapidly when ΔT is large. Although this crystallization rate may be reduced to some extent by decreasing the ΔT, the temperature control with small fluctuation was quite difficult in the time-resolved SAXS and FTIR measurements. Besides the temperature jump must be as sharp and stable as possible. Then the temperature-jump apparatus was designed carefully for this purpose. The details of the apparatus were already described in the previous article [17,23,24], except that an air bath was used instead of an oil bath to keep a sample at an isothermal crystallization temperature. The principle of this temperature jump was as follows: the sample holder was kept at first at the temperature above the melting point and then moved rapidly to another position controlled at a predetermined temperature (Tc). On the way of this rapid movement, the air was blown on the sample. This gave the very rapid cooling rate of ca. 600°C/min. Besides the temperature could be maintained at Tc with sufficiently small fluctuation. It should be emphasized here that the monitor of the sample temperature was quite important in this experiment. Therefore, we embedded the thermocouple inside the sample and monitored the temperature directly by recording on an x-y recorder. During this isothermal crystallization from the melt, time-resolved SAXS measurements were performed on the beam line #10C of the Photon Factory, High Energy Accelerator Research Organization, Tsukuba, Ibaraki, Japan. The wavelength of the incident X-ray beam was $\lambda = 1.4881$ Å. The sample-to-detector distance was 1900 mm. The scattered X-ray signal was detected by using a one-dimensional position sensitive proportional counter (PSPC) for the collection time of 3–7 s and at a time interval of 3–7 s. The scattering angle was calibrated by measuring the SAXS pattern of a dried hen collagen as a standard sample. The data correction was performed with respect to the background scattering and the fluctuation of incident beam intensity, followed by smoothing of the data.

3. Results and discussion

3.1. SAXS profile change

In the SAXS measurement, it is very important to check an effective range of the wave vector q, where

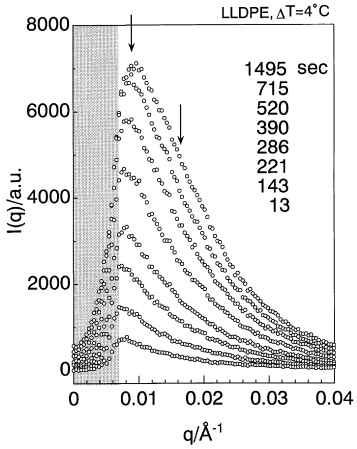

Fig. 2. Time dependence of the SAXS profile measured for LLDPE sample at the supercooling $\Delta T = 4$°C in the isothermal crystallization process from the melt.

$q = (4\pi/\lambda)\sin\theta$ (θ : scattering angle). In Fig. 1 SAXS profile of LLDPE sample is compared with that of a hen collagen, a standard sample. In the range of $q <$ ca. 0.0068 Å^{-1}, a masked region in Fig. 1, the SAXS intensity drastically decreases as a result of a beam stopper. Therefore, we may actually treat the SAXS data in the effective q range higher than 0.0068 Å^{-1}.

The time dependence of the SAXS intensity $I(q)$ measured for LLDPE sample during the isothermal crystallization at $\Delta T = 4$°C is shown in Fig. 2. In Fig. 3 is reproduced the time dependence of the SAXS profile measured for the DHDPE sample at $\Delta T = 4$°C. The experiments were made also under the other various ΔT conditions and all the SAXS data were found to show essentially the same time dependence. That is to say, these profile changes may be divided into three stages of time evolution.

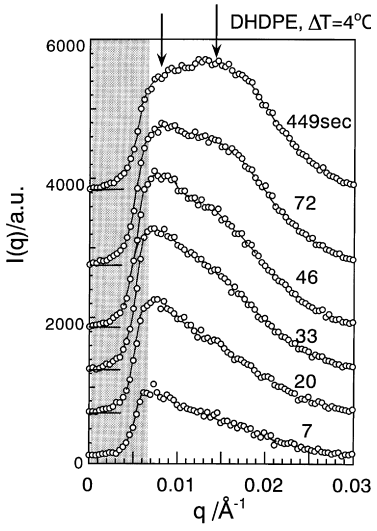

Fig. 3. Time dependence of the SAXS profile measured for DHDPE sample at the supercooling $\Delta T = 4$°C in the isothermal crystallization process from the melt.

(a) Time region I

LLDPE $\Delta T = 4$°C, $t = 0$–100 s
DHDPE $\Delta T = 4$°C, $t = 0$–20 s

After the sample was cooled rapidly to Tc from the melt, a Lorentzian-type SAXS profile appeared, whose peak was expected to be positioned at $q = 0$ Å^{-1}, and increased its intensity. This time region became shorter as the degree of supercooling was increased and also for the case of DHDPE than for LLDPE.

(b) Time region II

LLDPE $\Delta T = 4$°C, $t = 100$–220 s
DHDPE $\Delta T = 4$°C, $t = 20$–50 s

A peak began to be observed around $q = 0.008$ Å^{-1}, which corresponds to the periodic structure of ca. 700–800 Å, and increased its intensity with time.

(c) Time region III

LLDPE $\Delta T = 4$°C, $t = 220$ s
DHDPE $\Delta T = 4$°C, $t = 50$ s

As the time passed further, the position of this peak gradually shifted to higher q direction. This peak ceased the growth (for LLDPE, $\Delta T = 4$°C) or began to decrease the intensity (for DHDPE, $\Delta T = 4$°C). At the same time a shoulder began to appear around $q = 0.016$ Å^{-1} and increased the intensity in the case of LLDPE at $\Delta T = 4$°C, which corresponds to the long period of ca. 400 Å. In the case of DHDPE at $\Delta T = 4$°C, a clear peak was observed around $q = 0.013$ Å^{-1} and increased the intensity, during which the peak at $q = 0.008$ Å^{-1} decreased instead.

3.1.1. Time region I

In this time region, the SAXS intensity was observed apparently to increase gradually and monotonously. Then we assumed that this profile change may be interpreted on the basis of the thermal density fluctuation in the homogeneous system [28]. In this case the SAXS profile should take the Lorentzian-type shape with the peak at $q = 0$ Å^{-1}. Of course we can not say definitely whether the observed curves in this time range possess the peaks at center position or not, because we had the limited q range, as pointed out already. A possibility to detect another peak in the smaller q range will be discussed later. If the Lorentzian-type profile is assumed, then the Ornstein–Zernike (O–Z) plot is linear as expressed by the following equation;

$$1/I(q) = [1/I(0)][1 + q^2\xi^2] \quad (1)$$

where $I(0)$ is the scattering intensity and ξ is the correlation length. As a typical example, the case of LLDPE at $\Delta T = 4$°C will be shown here. (In the case of DHDPE at $\Delta T = 4$°C, this time region is too narrow and is not practical for the quantitative discussion.) In Fig. 4 are shown the O–Z plots made for the LLDPE ($\Delta T = 4$°C) in the time region where no peak could be observed in the SAXS profiles. In the q

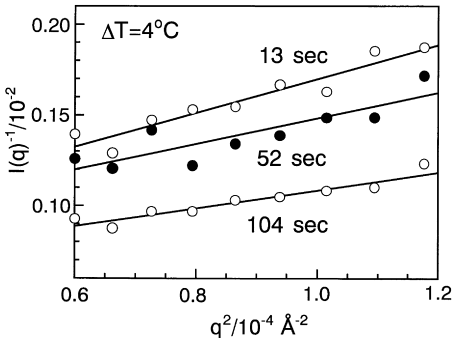

Fig. 4. Ornstein–Zernike plot for LLDPE sample in the time region of the earliest stage of the isothermal crystallization from the melt ($\Delta T = 4$°C).

range smaller than Rg^{-1}, where Rg is the radius of gyration of the random coil (=130 Å according to the small-angle neutron scattering measurement [25,29]), the O–Z plot was found to be linear, supporting the reasonableness of the interpretation based on the homogeneous one-phase system [30]. It should be noticed here that the O–Z plot was made in a relatively narrow q range because of the limitation caused by the effect of X-ray beam stopper, and so the linear relation between $1/I(q)$ vs. q^2 might be only apparent. But the linear relation itself between $1/I(q)$ and q^2 was not inconsistent with the assumption that the SAXS profile was similar to that expected from the thermal density fluctuation. Another possibility will be discussed in a later section. The $1/I(0)$ and ξ could be obtained by plotting $1/I(q)$ against q^2. In Fig. 5, $1/I(0)$ and ξ estimated from Fig. 4 are plotted against time. In the early stage of the crystallization of LLDPE at $\Delta T = 4$°C, the $I(0)$ increased with time and was predicted to be diverged into infinity around 210 s, as estimated from the extrapolation of the $1/I(0)$ to the zero value. But, in the actual system, before being diverged into infinity, the other type of structural change began to occur around 100 s, and so the treatment of the data on the basis of the O–Z plot could not be useful anymore.

The ξ value, 70–80 Å, is consistent with the correlation length predicted from such a model that the random coils of ideal state (Gaussian chains) are mixed together

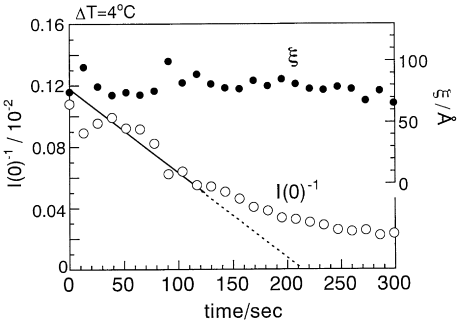

Fig. 5. Time evolution of $1/I(0)$ and the correlation length ξ obtained from the Ornstein–Zernike plot for LLDPE sample in the time region of the earliest stage of the isothermal crystallization from the melt ($\Delta T = 4$°C). Refer to Fig. 4.

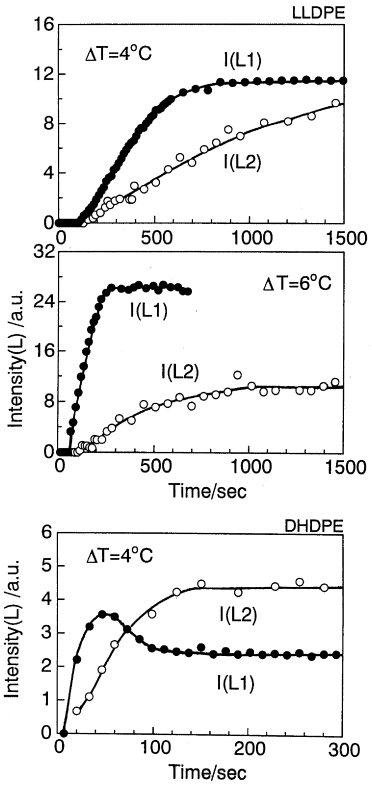

Fig. 6. Time dependence of the peak intensities evaluated from the SAXS data of LLDPE sample ($\Delta T = 4$ and 6°C) and DHDPE sample ($\Delta T = 4$°C). The L_1 and L_2 correspond to the peaks observed in the early and the later stages of isothermal crystallization. Refer to Figs. 2 and 3.

homogeneously. In this model the correlation length is given theoretically as $\xi = Rg/\sqrt{3} = 75$ Å, where the radius of gyration of the chain Rg = ca. 130 Å [29,30]. The value is almost in agreement with that shown in Fig. 5. This result is also consistent with the experimental data of small-angle neutron scattering collected for the blends of deuterated and hydrogenous PEs, revealing the reasonableness of an assumption of homogeneously mixed Gaussian-type chains in the molten state [29]. This random-coil character is assumed to be held even in the time region I, giving the earlier-mentioned good relation in the correlation length between the observed and calculated values. In this way, the O–Z plot made in this time region may be assumed to be reasonable although the available q range is narrow as pointed out earlier.

3.1.2. Time regions II and III

In this time region, a peak began to be detected at ca. $q = 0.008$ Å^{-1} and increased its intensity with time, implying the appearance of a periodic structure of 700–800 Å. Fig. 6 shows the time evolution of the peak intensities $I(L_1)$ and $I(L_2)$ of the periodic structures of $L_1 = 800$ Å and $L_2 = 400$ Å, where the $I(L_1)$ was estimated directly from Figs. 2 and 3, while the $I(L_2)$ was obtained from the data analysis based on the correlation function as will be mentioned in a later section. As a trial, the logarithm $I(q)$ at a constant q

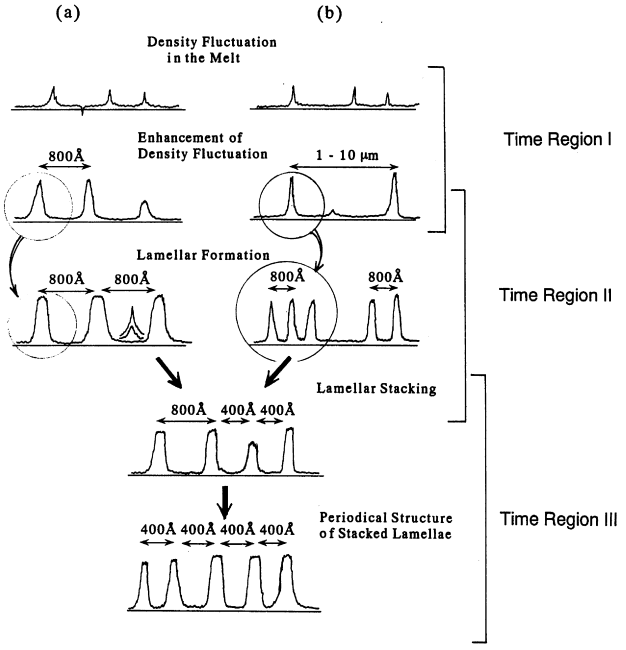

Fig. 7. An illustrated structural change of PE in the isothermal crystallization from the melt: (a) The density fluctuation in the melt develops to the isolated lamellar structure of ca. 800 Å period; (b) The density fluctuation in the melt develops to the separated regions of high and low density with a period of 1 μm order. In the high-density region, the lamellar stacking occurs with ca. 800 Å period. It should be noticed that the scale is quite different between the models (a) and (b). In both the models (a) and (b), the lamellar structure of 800 Å period becomes more highly densed stacking structure of ca. 400 Å period by introducing new lamellae in between the already existing lamellar layers. In the case of LLDPE, this structural change ceased on the way and both the periods of 400 and 800 Å coexisted, while it was completed for the case of DHDPE.

position was plotted against time. This plot was found to be apparently linear in the time region of 100–220 s; i.e., $I(q)$ is expressed by an exponential form of time. This behavior of $I(q)$ is apparently similar to the spinodal decomposition observed for polymer alloy [31,32]. But, in general, the concept of spinodal decomposition is applied to the case where the so-called conservation law is held in the system [33–35]. The observation of the long period at $q = 0.008\ \text{Å}^{-1}$ suggests the drastic change in the order parameter necessary for the description of the structural transition in the crystallization process (or non-conservation of the order parameter before and after the transition). That is to say, the observation of the long period does not seem to match to the concept of spinodal decomposition in these time regions. Rather, judging from the S-shaped curve of $I(q)$ vs time plot seen in Fig. 6, which is similar to the curve expected from the so-called Avrami equation as shown in a later section, it might be reasonable to assume an occurrence of nucleation and growth of the crystalline lamellae in these time regions II and III. The quantitative analysis will be made in a later section.

In the later part of the time region II, the peak of the SAXS profile shifted from ca. 0.008 Å^{-1} to higher q value as seen in Figs. 2 and 3, indicating that the structural period became apparently shorter. The intensity of this peak increased still but the increasing rate became slower. As the time passed further, a new phenomenon began to be observed. That is, a shoulder (for the case of LLDPE at $\Delta T = 4$°C) or a peak (for the case of DHDPE at $\Delta T = 4$°C) began to appear around $q = 0.016\ \text{Å}^{-1}$ and increased the intensity gradually. At the same time the original peak of 800 Å period ceased to increase (for LLDPE with $\Delta T = 4$°C) or decreased gradually (for LLDPE at $\Delta T = 6$°C and DHDPE at $\Delta T = 4$°C), as shown in Fig. 6. This new peak corresponds to the periodical structure of ca. 400 Å (L_2). In this way, in the crystallization of PE, the periodic structure of about 800 Å changed gradually into the periodic structure of 400 Å. In more detail, the 400 Å periodical structure coexists with the 800 Å periodical structure in the case of LLDPE at $\Delta T = 4$°C, while the 400 Å structure increases the population and the 800 Å structure decreases the population in the case of DHDPE at $\Delta T = 4$°C. From these observations, we may speculate that a new lamella is generated between the already existing lamellae of 800 Å period and the lamellar stacking structure takes ca. 400 Å period.

Based on the interpretation made for the time regions I–III, a schematic illustration of lamellar growth mechanism is shown in Fig. 7 (a). Immediately after the temperature jump is completely finished, the density fluctuation is enhanced in the melt, giving an increase of SAXS intensity (Time region I). As the time passes, this density fluctuation is increased further and the higher density part is speculated to concentrate into a crystal nucleus (Time region II). Staring from

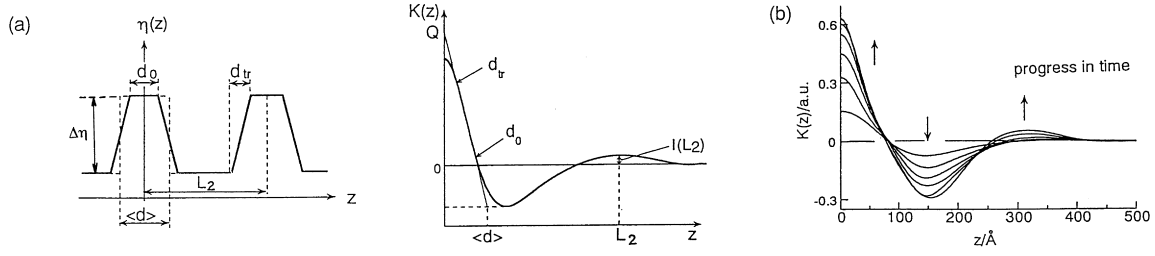

Fig. 8. (a) The electron density correlation function $K(z)$ and the electron density distribution $\eta(z)$ for the lamellar system. Q: the invariant, d_{tr}: thickness of the transition zone between the crystalline lamella and amorphous part, d_o: thickness of lamellar core, $< d >$: mean lamellar thickness, L_2: long-period, and $I(L_2)$: electron density difference between crystalline lamella and amorphous part; (b) Example of time evolution of $K(z)$.

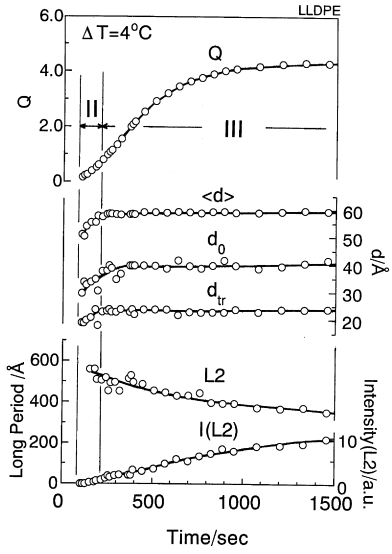

Fig. 9. Time dependence of the various parameters obtained by the calculation of correlation functions from the SAXS profiles of LLDPE sample measured in the isothermal crystallization from the melt at $\Delta T = 4$°C.

these nuclei, the lamellar structure of the period of 700–800 Å is created. These lamellae are considered to be isolated from each other by an amorphous region because the lamellar thickness estimated from the correlation function analysis, as will be described later, is only 60 Å. With a passage of time, the period decreases gradually. At the same

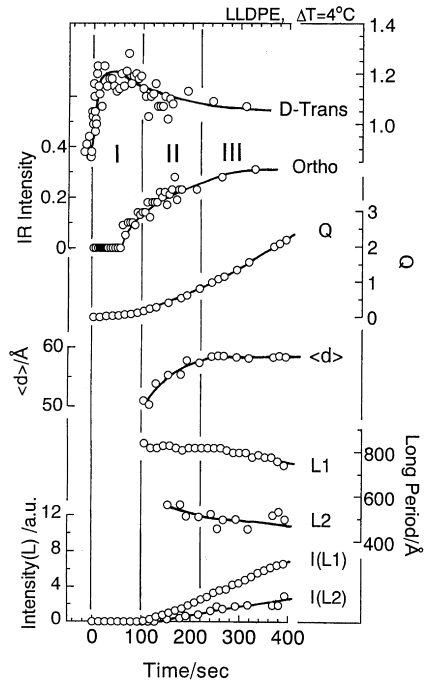

Fig. 10. Combination of the vibrational spectroscopic data with the SAXS data collected for the LLDPE sample in the isothermal crystallization process from the melt at $\Delta T = 4$°C. Q: invariant, $\langle d\rangle$: lamellar thickness. L_1 (800Å) and L_2 (400 Å) denote, respectively, the long spacings of the lamellar stacking structure. $I(L_1)$ and $I(L_2)$ denote the intensities measured for the SAXS peaks corresponding to these periods.

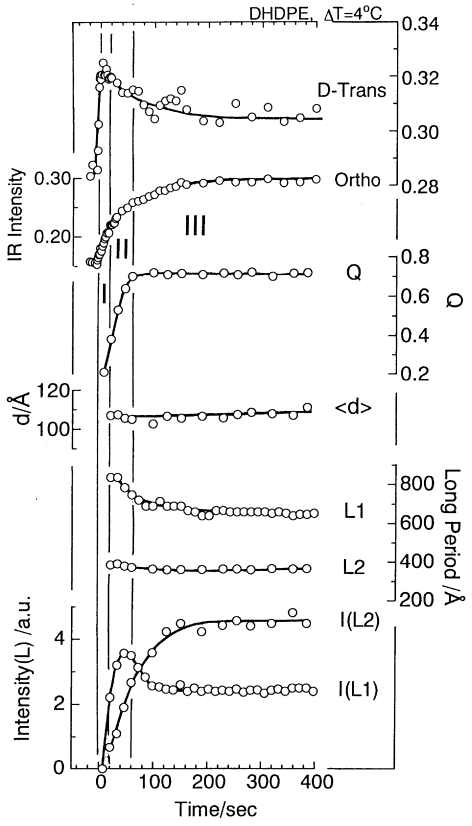

Fig. 11. Combination of the vibrational spectroscopic data with the SAXS data collected for the DHDPE sample in the isothermal crystallization process from the melt at $\Delta T = 4$°C. Q: invariant, $\langle d\rangle$: lamellar thickness. L_1(800Å) and L_2(400Å) denote, respectively, the long spacings of the lamellar stacking structure. $I(L_1)$ and $I(L_2)$ denote the intensities measured for the SAXS peaks corresponding to these periods.

time, between these isolated lamellae, new lamellae are generated and the structure changes gradually into more densely stacked lamellar structure of the long period of ca. 400 Å (Time region III). In the case of LLDPE at $\Delta T = 4$°C, this structural change was not completed in the experimental time range but it almost finished in the case of DHDPE at $\Delta T = 4$°C as seen in Fig. 6.

3.2. Correlation function and the structure parameters

The one-dimensional electron-density correlation function *K(z)* was calculated from the SAXS data. Under the assumption of the two-phase model consisting of the alternately stacked structure of the crystalline and amorphous layers, the *K(z)* is defined by the following equation [36,37].

$$K(z) = \langle [\eta(z') - \langle\eta\rangle][\eta(z+z') - \langle\eta\rangle]\rangle$$

$$= 2\int_0^\infty (\pi)^{-1} q^2 I(q)\cos(qz)\,dq \qquad (2)$$

where $\langle\ \rangle$ is the statistical average and $\eta(z)$ and $\langle\eta\rangle$ are the electron density variation along the lamellar normal and the mean electron density, respectively. Various points

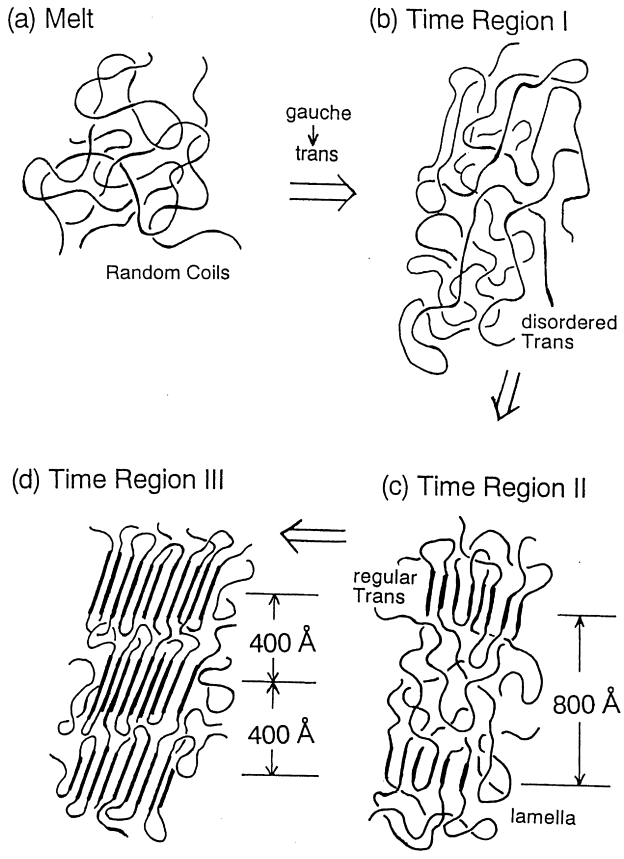

Fig. 12. Illustration of structural change in the isothermal crystallization of PE. The case of model (a) in Fig. 10 is described in more details based on the combined data of SAXS and FTIR (refer to the text).

indicated on the *K(z)* curve give various physical parameters as shown in Fig. 8(a): the invariant $Q = \int_0^\infty (\pi)^{-1} q^2 I(q)\, dq$, the mean lamellar thickness $\langle d \rangle$, the mean boundary thickness d_{tr}, the mean core thickness d_0, and the long spacing L_2 [36,37].

It should be noticed here that the *K(z)* can be used for the crystallization stages of II and III because the two phase structure is attained in these time regions. Fig. 8 (b) shows the example of the time evolution of *K(z)* calculated for the LLDPE at $\Delta T = 4$°C. In Fig. 9 is shown the time dependence of the structural parameters of LLDPE obtained from the *K(z)* curves. After the temperature jump, the invariant *Q* increased gradually, reflecting the increase of the thermal density fluctuation. The parameters related with the lamellar thickness d_{tr}, d_0 and $\langle d \rangle$ increased to ca. 25, 40 and 60 Å, respectively, at $t = 150$ s and became almost constant afterwards. In the time region II, the peak L_1 corresponding to the initially-observed peak in Fig. 2 was difficult to detect in the *K(z)* curve. The peak of the long period (L_2) reflecting the lamellar stacking structure began to appear in the time region III and decreased the value gradually to ca. 350 Å. The peak height $I(L_2)$ evaluated from the *K(z)* at $z = L_2$ position increased correspondingly, indicating the increase of the electron density difference between the crystalline lamella and the amorphous phase.

3.3. Details of structural changes viewed from the coupled data of FTIR and SAXS

In the previous article we reported the time resolved FTIR measurements made in the isothermal crystallization process of PE, from which the ordering process of the chain conformation was proposed [17]. As the two kinds of data, FTIR and SAXS are now combined to get more concrete structural change of the chains in this crystallization process.

In Figs. 10 and 11, the time dependencies of the lamellar structural parameters obtained from the SAXS data are compared with those of the IR band intensities estimated, respectively, for the three cases: LLDPE ($\Delta T = 4$°C) and DHDPE ($\Delta T = 4$°C). This comparison can be made reasonably because the temperature jump in both the measurements was carried out at almost the same rate of ca. 600°C/min. The structural change deduced from the following discussion is illustrated schematically in Fig. 12.

3.3.1. (1) Time region I

In this time region, the 1368 cm^{-1} IR band (LLDPE) or the 1089 cm^{-1} band (DHDPE) increased the intensity remarkably and kept the intensity for a while, which are characteristic of the disordered *trans* form. Correspondingly the thermal density fluctuation was observed in the SAXS measurement, giving a gradual increase of the invariant *Q*. From these data, we may have an image that the transformation from *gauche* to *trans* conformers occur drastically in the random coils during the earliest stage of crystallization, giving an increase of density fluctuation in the homogeneous system. After that, the disordered *trans* band began to decrease in intensity and the IR band of regular *trans*-zigzag form increased the intensity, and around here the invariant *Q* began to accelerate the growing rate.

3.3.2. Time region II

The enhancement of density fluctuation between the *gauche* and the disordered *trans* segments resulted in the formation of a nucleus in which the regular *trans*-zigzag chain segments were aggregated together to form a lamellar sheet of ca. 50 Å thickness. The increase of intensity of IR band characteristic of regular *trans*-zigzag form was accelerated further. That is, the formation of isolated lamellae was accelerated and the periodic structure was formed with a period of ca. 800 Å.

3.3.3. Time region III

In this region, new lamellae were created in between the already existing lamellae and the more densely stacked lamellar structure was constructed with a long period of ca. 400 Å. This structural ordering occurs enough well in the case of DHDPE (Fig. 6) but the original 800 Å period structure remains appreciably in the case of LLDPE sample.

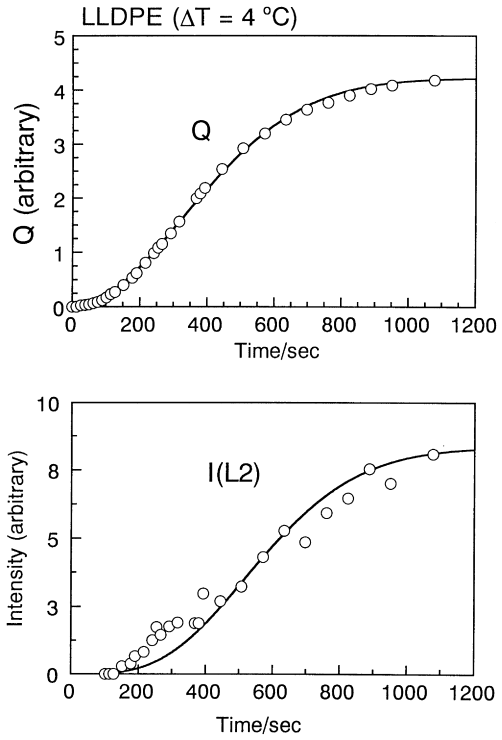

Fig. 13. Time evolutions of the invariant Q (upper) and the SAXS intensity of the long period L_2 (lower) measured for LLDPE sample at $\Delta T = 4$°C. The solid curves are calculated on the basis of Avrami equation for the nucleation and growth of crystalline lamellae.

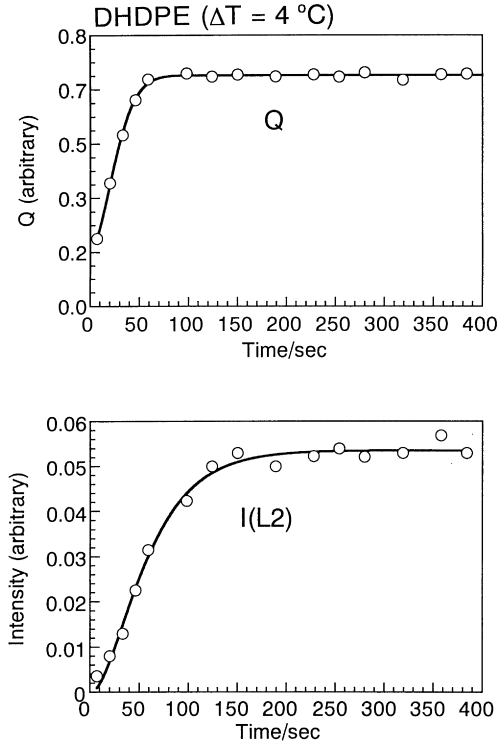

Fig. 14. Time evolutions of the invariant Q (upper) and the SAXS intensity of the long period L_2 (lower) measured for DHDPE sample at $\Delta T = 4$°C. The solid curves are calculated on the basis of Avrami equation for the nucleation and growth of crystalline lamellae.

3.3.4. Analysis of time-dependence of SAXS profiles

The SAXS profiles observed in these time regions II and III are now tried to be interpreted on the basis of an idea of nucleation and growth of the crystalline lamellae. As already mentioned, the time evolution of the SAXS intensity of the 800 Å peak (Fig. 6) and that of the invariant Q (Figs. 10 and 11) show the curves similar to that expected from the Avrami equation [38,39]. Let us assume here that (i) the disordered *trans* segments grown in time region I are gathered together and regularized to the crystalline nucleus consisted of extended planar-zigzag segments of orthorhombic-type packing structure, and (ii) these nuclei grow into larger lamellae with ca. 800 Å long period, and further to those of 400 Å period. (Of course, these assumptions should be confirmed by the observation of the nucleation and growth of spherulites through the optical microscope or light scattering technique or wide-angle X-ray scattering measurement, which will be made as a future research theme.) Based on these assumptions the invariant Q evaluated in Figs. 10 and 11 may be expressed by the following equations in the time regions II and III. As

$$Q \propto X_c(1 - X_c) \approx X_c \qquad (X_c \ll 1) \tag{3}$$

where X_c is the degree of crystallinity, and

$$X_c = 1 - \exp(-k \cdot t^n) \tag{4}$$

where k is a constant and n is the Avrami index, and then we have

$$Q \propto 1 - \exp(-k \cdot t^n) \tag{5}$$

Eqs. 4 and 5 contain both the contribution from nucleation and growth of the crystals. Ideally we should separate these two contributions in the interpretation of the time evolution of the SAXS data, but the separation was quite difficult in the treatment of the experimental data obtained in the present research, being one of the reasons why the Avrami equation was employed here. Based on Eq. 5, the Q data were fitted reasonably by assuming the following parameters (see Figs. 13 and 14).

For LLDPE ($\Delta T = 4$°C), $k = 6.99 \times 10^{-6}$ and $n = 1.93$
For DHDPE ($\Delta T = 4$°C), $k = 0.0025$ and $n = 1.75$

These values of n seem reasonable when compared with those of PE samples reported in the Refs [40–43].

In the time regions II and III we assumed the two-phase model consisted of the lamellar and amorphous regions, as already discussed in the previous section. If the thickness of the transition zone between the crystalline and amorphous regions is neglected (Fig. 8), then the SAXS peak intensity $I(q_{max})$ can be expressed as follows in a good approximation [44].

$$I(q_{max}) = |F|^2 S^2 \propto \langle d \rangle^2 (\Delta\eta)^2 \left[1 - \left(\langle d \rangle^2 l^2/48\right) q_{max}^2\right] N^2 \tag{6}$$

$$\propto X_c^2 \left[1 - \left(\langle d \rangle^2 l^2/48\right) q_{max}^2\right]$$

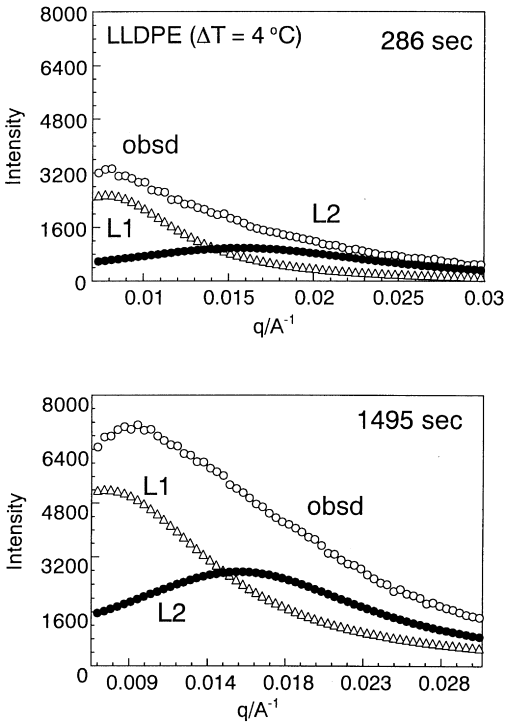

Fig. 15. SAXS profiles and their components of the long period structures L_1 and L_2 evaluated for the data at the different time of the LLDPE sample ($\Delta T = 4$°C).

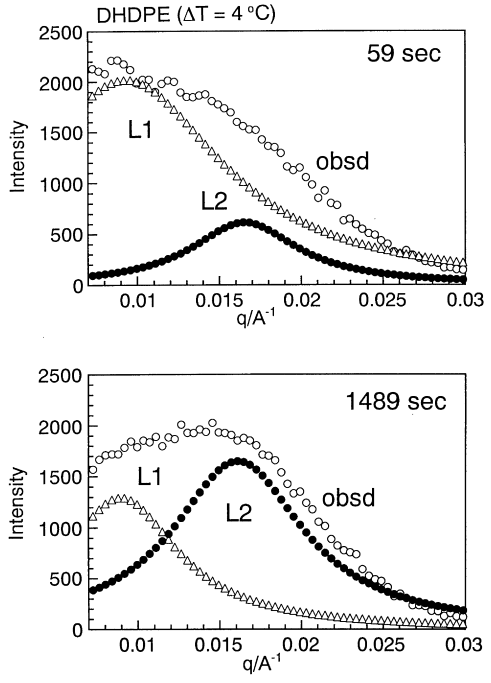

Fig. 16. SAXS profiles and their components of the long period structures L_1 and L_2 evaluated for the data at the different time of the DHDPE sample ($\Delta T = 4$°C).

where F is the structure factor of this two-phase system and S is the form factor introduced for the assumption of finite array of N stacked lamellae. The $\langle d \rangle$ is the mean lamellar thickness, $\Delta\eta$ is the difference in the density between the crystalline and amorphous regions, and l is the scattering order ($l = 1$ in the present study). The q_{max} is the q vector corresponding to the SAXS peak. In order to distinguish the two peaks (L_1 and L_2), the notations $q_{max}^{L_1}(= 2\pi/L_1)$ and $q_{max}^{L_2}(= 2\pi/L_2)$ are used here. The increase in the SAXS intensity may be reproduced by assuming the time evolution of the lamellar thickness $\langle d \rangle$, the number of stacked lamellae N, and the electron density difference $\Delta\eta$. In the one-dimensional two-phase model, the degree of crystallinity is given by $X_c = \langle d \rangle / L$. But the actually the crystallinity may increase in a complicated manner not only by the increase of $\langle d \rangle$ but also by the increase of N and so on. The second equation in Eq. 6 is given under such an assumption. By taking into consideration this situation of the structural change, the SAXS intensities of the L_1 and L_2 peaks may be written approximately in the following equations.

$$I(L_1) = I(q_{max}^{L_1}) \propto X_c(L_1)^2 \left[1 - \left(\langle d \rangle^2 l^2 / 48 \right) \left(q_{max}^{L_1} \right)^2 \right] \tag{7}$$

$$I(L_2) = I(q_{max}^{L_2}) \propto X_c(L_2)^2 \left[1 - \left(\langle d \rangle^2 l^2 / 48 \right) \left(q_{max}^{L_2} \right)^2 \right] \tag{8}$$

where the $X_c(L_i)$ ($i = 1$ and 2) denotes the degree of crystallinity contributed by the structure of the long period L_i. The time dependence of X_c was given by Eq. 4 as the following:

$$X_c(L_1) \propto 1 - \exp(-k_1 n_1) \tag{9}$$

(in Time region II)

$$X_c(L_2) \propto 1 - \exp[-k_2 (t - t_0)^{n_2}] \tag{10}$$

(in Time region III)

$$X_c(L_1) \propto 1 - X_c(L_2) \propto \exp[-k_2 (t - t_0)^{n_2}]$$

(in Time region III)

where the $X_c(L_1)$ is considered to decrease in the time region III because of the increase of the structure of long period L_2. The t_o is used to indicate the time lag between the appearance of the peaks L_1 and L_2. In the actual data analysis we assumed simply that $k_1 = k_2 = k = 6.99 \times 10^{-6}$ and $n_1 = n_2 = n = 1.93$ for LLDPE ($\Delta T = 4$°C) and $k_1 = k_2 = k = 0.0025$ and $n_1 = n_2 = n = 1.75$ for DHDPE ($\Delta T = 4$°C).

Our purpose is to check whether the SAXS data obtained in the time regions II and III can be reproduced reasonably or not by Eqs. 7–10. The time evolution of the peak intensity $I(L_2)$ of the long period L_2 was presented in Figs. 10 and 11, which was evaluated from the correlation function (see Fig. 8) and may be considered to reflect relatively well the original contribution of the pure L_2 structure. Moreover, $I(L_1)$ of the long period L_1 was estimated directly from

Figs. 2 and 3 without any curve separation process, and so the contribution from $I(L_2)$ seems to be included more or less, as already explained earlier. Therefore we tried to fit the $I(L_2)$ data at first in order to adjust the parameters (k and n) and then to reproduce the total SAXS profiles contributed from both the L_1 and L_2 structures.

The curve fittings of $I(L_2)$ made for the cases of LLDPE and DHDPE are shown in Figs. 13 and 14, respectively. The used parameters in Eqs. 7 and 8 were $\langle d \rangle = 60$ Å (for LLDPE, Fig. 10) and 110 Å (for DHDPE, Fig. 11) and $q_{\max}^{L_2} = 400$ (for LLDPE) and 380 Å (for DHDPE). The k values were transferred directly from the data analysis of the invariant Q. The thus adjusted parameter n was 1.91 for LLDPE and 1.56 for DHDPE. They are relatively close to those determined from the Q data. The time lag t_0 was found to be almost 0, indicating that immediately after the appearance of the 800 Å long period structure, the 400 Å periodic structure begins to appear in some parts and grows even in the early stage of crystallization in the actual samples.

As the next step, the observed SAXS profiles were tried to be reproduced on the basis of the following equations combined with Eqs. 7–10.

$$I(q) = wI(q^{L_1}) + (1 - w)I(q^{L_2}), \tag{11}$$

$$I(q^{L_1}) = I(q_{\max}^{L_1}) / \left[(q - q_{\max}^{L_1})^2 + \Delta_{L_1}^2 \right], \tag{12}$$

$$I(q^{L_2}) = I(q_{\max}^{L_2}) \left[(q - q_{\max}^{L_2})^2 + \Delta_{L_2}^2 \right]. \tag{13}$$

In these equations, the Lorentz-type functions were assumed for the SAXS profiles. The Δ_L is the width of the profile. Figs. 15 and 16 show the results made for LLDPE and DHDPE at $\Delta T = 4$°C, respectively, where the components of the L_1 and L_2 peaks are also indicated. These figures allow us to recognize the following tendency that, during the crystallization process in the time regions II and III, the SAXS components originating from the 800 Å period begins to appear and increase the peak height and decreases again, just when the SAXS component of the 400 Å periodic structure appears and grows its population with time.

In this way, by assuming the evolution of the 800 Å and 400 Å periodic structure of repeatedly stacked lamellae, the time dependencies of the SAXS data including the Q, $I(L_1)$, $I(L_2)$ and the profile itself could be reasonably interpreted on the basis of an idea of the nucleation and growth of the lamellar structure. The nucleation may correspond to the regularization of the disordered *trans* segments to the orthorhombic-type structure, as speculated already from the clear intensity exchange between the IR bands (Figs. 10 and 11) and the time evolution of the invariant Q. However, the growth of these orthorhombic-type lamellae with the stacking structure reflects on the complicated change in the SAXS patterns in the time regions II and III.

3.4. A possibility of another model

At this stage, we need to remember the discussion made in the section of SAXS data treatment. Concerning the SAXS data in the time region I, we did not have any information whether any additional peak appeared or not in the low q range. We assumed that the SAXS profile exhibited the peak only at the center position of $q = 0$ Å^{-1} and that the O–Z plot based on the density fluctuation in the homogeneous system could be usefully applied to the analysis of the SAXS profile observed in this time region. But, in the crystallization phenomenon, we always have to take the spherulite structure into consideration, which can be obtained in the sample crystallized from the melt. In general, the distance between the adjacent spherulites is an order of μm, corresponding to the q value of 10^{-3} Å^{-1} order. Stein et al. measured the small-angle light scattering and SAXS in the course of crystallization of PE and proposed that the shell of spherulites was formed at the early stage of the crystallization [11,12,45]. If this is true, then it might be assumed that the peak corresponding to $q \sim 10^{-3}$ Å^{-1} should appear in the scattering experiment before the already-mentioned peak is observed at $q = 0.008$ Å^{-1} (800 Å period) [46]. Besides we can not analyze anymore the data in this time region on the basis of the O–Z approximation.

According to this prediction, another schematic image may be proposed for the PE crystallization as shown in Fig. 7 (b). Immediately after the temperature-jump, the conformationally disordered *trans* form is induced with a period of μm. In the domain of disordered *trans* segments, the disorder-to-order conformational transition occurs and the disordered *trans* region and the regular *trans* region coexist with 800 Å period. The regular *trans* segments are gathered to form the orthorhombic crystalline lamella and develop to more densely stacked lamellar structure of ca. 400 Å period.

In order to check which structural models are more suitable for the crystallization mechanism of PE, we need to measure the ultra-low q range of ca. 10^{-3} Å^{-1} by using some other techniques such as small-angle light scattering etc. in addition to the direct observation of crystal growth by optical microscopy [46].

References

[1] In: Dasiere M, editor. Proceedings of the NATO advanced research workshop on crystallization of polymers, 405. Dordrecht: Kluwer Academic Publishers, 1993 Series C.
[2] Ungar G, Keller A. Polymer 1986;27:1835.
[3] Barham PJ, Keller A. J Polym Sci Part B: Polym Phys 1989;27:1029.
[4] Rastogi S, Hikosaka M, Kawabata H, Keller A. Macromolecules 1991;24:6384.
[5] Hikosaka MJ. Macromol Sci-Phys 1992;B31:87.
[6] Rastogi S. Prog Colloid Plym Sci 1992;87:42.
[7] Schultz JM. J Polym Sci: Polym Phys Ed 1976;14:2291.
[8] Schultz JM, Lin JS, Hendricks RW. J Appl Crystallogr 1978;11:551.

[9] Strobl GR. Schneider M. Macromolecules 1980;18:1343.
[10] Albrecht T, Strobl GR. Macromolecules 1996;29:783.
[11] Song HH, Stein RS, Wu DQ, Ree M, Phillips JC, LeGrand A, Chu B. Macromolecules 1988;21:1180.
[12] Song HH, Wu DQ, Satkowski M, Ree M, Stein RS, Phillips JC. Macromolecules 1990;23:2380.
[13] Russell TP, Koberstein JT. J Polym Sci: Polym Phys Ed 1985;23:1109.
[14] Yoshida H. Thermochim Acta 1995;264:173.
[15] Tashiro K. Acta Polymer 1995;46:100.
[16] Tashiro K, Sasaki S, Kobayashi M. Macromolecules 1996;29:7460.
[17] Tashiro K, Sasaki S, Kobayashi M. Polym J 1998;30:485.
[18] Tashiro K, Stein RS, Hsu SL. Macromolecules 1992;25:1801.
[19] Tashiro K, Satkowski MM, Stein RS, Li Y, Chu B, Hsu SL. Macromolecules 1992;25:1809.
[20] Tashiro K, Izuchi M, Kobayashi M, Stein RS. Macromolecules 1994;27:1221.
[21] Tashiro K, Izuchi M, Kobayashi M, Stein RS. Macromolecules 1994;27:1228.
[22] Tashiro K, Izuchi M, Kobayashi M, Stein RS. Macromolecules 1994;27:1234.
[23] Tashiro K, Izuchi M, Kaneuchi F, Jin C, Kobayashi M, Stein RS. Macromolecules 1994;27:1240.
[24] Tashiro K, Imanishi K, Izumi Y, Kobayashi M, Kobayashi K, Satoh M, Stein RS. Macromolecules 1995;28:8477.
[25] Tashiro K, Imanishi K, Izuchi M, Kobayashi M, Itoh Y, Imai M, Yamagichi Y, Ohashi M, Stein RS. Macromolecules 1995;28:8484.
[26] Hoffman JD, Weeks JJ. J Res Natl Bur Stand: Part A 1966;66:13.
[27] Alamo RG, Viers BD, Mandelkern L. Macromolecules 1995;28:3205.
[28] Hashimoto T, Izumitani T, Takenaka M. Macromolecules 1989;22:2293.
[29] Tashiro K, Sasaki S, Imai M, Yamagichi Y, Ohashi M. Activity Report on Neutron Scattering Research 1997;4:195.
[30] de Gennes PG. Scaling concepts in polymer physics. Ithaca, NY: Cornell University Press, 1979.
[31] Cahn JW, Hillard JE. J Chem Phys 1958;28:258.
[32] de Gennes PG. J Chem Phys 1980;72:4756.
[33] Imai M, Mori K, Mizukami T, Kaji K, Kanaya T. Polymer 1992;33:4451.
[34] Imai M, Kaji K, Kanaya T. Macromolecules 1994;27:7103.
[35] Imai M, Kaji K, Kanaya T, Sakai Y. Phys Rev B 1995;52:12696.
[36] Strobl GR, Schneider M. J Polym Sci: Polym Phys Ed 1980;18:1343.
[37] Strobl GR, Schneider M, Voiget-Martin IG. J Polym Sci: Polym Phys Ed 1980;18:1343.
[38] Schultz JM. Polymer materials science. Englewood Cliffs, NJ: Prentice-Hall, 1974.
[39] Sharples A. Introduction to polymer crystallization. London: Edward Arnold Limited, 1966.
[40] Banks W, Gordon M, Roe RJ. Sharples. A. Polymer 1963;4:61.
[41] Schultz JM, Scott RD. J Polym Sci: Part A-2 1969;7:659.
[42] Schultz JM, Lin JS, Hendricks RW. J Appl Cryst 1978;11:551.
[43] Polymer handbook. In: Brandrup J, Immergut EH, editors. 3. New York: Wiley Interscience, 1989. p. VI.
[44] Strobl GR, Ewen B, Fischer EW, Piesczek W. J Chem Phys 1974;61:5257.
[45] Stein RS, Cronauer J, Zachmann HG. J Macromol Structure 1996;383:19.
[46] Kaji K. Private communication.